Robotica (2012) volume 30, pp. 989–1003. © Cambridge University Press 2011
doi:10.1017/S0263574711001226

Limit cycle walking, running, and skipping of telescopic-legged rimless wheel

Fumihiko Asano* and Masashi Suguro

School of Information Science, Japan Advanced Institute of Science and Technology, 1-1 Asahidai, Nomi, Ishikawa 923-1292, Japan

(Accepted October 27, 2011. First published online: November 29, 2011)

SUMMARY

This paper investigates the efficiency and properties of limit cycle walking, running, and skipping of a planar, active, telescopic-legged rimless wheel. First, we develop the robot equations of motion and design an output following control for the telescopic-legs' action. We then numerically show that a stable walking gait can be generated by asymmetrizing the impact posture. Second, we numerically show that a stable running gait can be generated by employing a simple feedback control of the control period, and compare the properties of the generated running gait with those of the walking gait. Furthermore, we find out another underlying gait called skipping that emerges as an extension of the walking gait. Through numerical analysis, we show that the generated skipping gaits are inherently stable and are less efficient than the other two gaits.

KEYWORDS: Gait generation; Limit cycle walking; Running; Skipping; Telescopic-legged rimless wheel.

1. Introduction

Legged robots based on passive dynamics are called "limit-cycle walkers" and are believed to be the leading candidate for achieving natural, efficient, and human-like legged locomotion robots. Stable gaits of limit-cycle walkers are generated as a limit cycle including a state jump caused by the collision of the stance-leg exchange. It is well known that limit-cycle walkers including passive-dynamic bipeds[1] can easily generate stable gaits by setting suitable system parameters and initial conditions. This is because the walking gaits are inherently stable. The underlying self-stabilization principle is, however, still unclear and is expected to be mathematically proved.

Robotic dynamic running is also one of the most active topics in the field of the limit-cycle walkers. Limit-cycle running is necessary for expanding the potentiality of efficient legged locomotion that adopts various unknown environments while changing the gait patterns. Unlike the walking gaits, however, the running gaits include flight phases in the limit cycle, and generating stable running gaits is thus more difficult due to the highly dynamic motion.

In human walking, the change rate of metabolic energy cost radically changes to decrease when exceeding the highest walking speed; this is produced by changing the gait from walking to running.[2] It is believed that, in high-speed locomotion, humans prefer running to walking for energy saving. Ponies also change their gait from walking to trotting or to galloping as the moving speed increases. At every transition point, the change rate of metabolic cost dramatically decreases. Our study on limit-cycle runners is motivated by the desire to achieve more efficient and more high-speed legged locomotion, and by the policy that changing to running is more natural than maintaining inefficient high-speed walking.

Robotic dynamic runners usually utilize the compliance of the lower limb.[3–5] Unlike previous studies, however, the authors consider a robotic runner without having leg compliance; the robot achieves active dynamic running only by the effect of high-speed telescopic-legs' actuation. Using this model, we try to generate high-speed running gaits that emerge as a natural extension of the walking gait.

Several methods for generating level gaits of limit-cycle walkers have been proposed and have successfully been applied.[9] It has already been shown theoretically and experimentally that achieving efficient level walking is not difficult if negative actuator work can be avoided. We have also proposed a novel method for generating high-speed level gaits of limit-cycle walkers utilizing the telescopic-legs' action.[6,7] The primary purpose of this approach is to make overcoming the potential barrier at midstance easy by tilting the robot's impact posture forward. The robot lengthens the stance leg while shortening the swing leg during the stance phase for creating the next impact posture, and the mechanical energy is accordingly restored. This approach is very useful for generating high-speed level gaits of the telescopic-legged rimless wheels as well as bipedal walkers.[8] The ground reaction force, however, often becomes negative in return for the high-speed stance-leg extension.[6] The robot would jump or should change motion to the running gait in this case.

In this paper, we deal with the model of a telescopic-legged rimless wheel that consists of eight identical telescopic legs for analysis. We first describe the robot equations of motion and outline the walking gait generation based on asymmetrization of the impact posture. Next, we numerically show that a stable running gait can be generated by shortening the control period for the telescopic-legs' action, that the generated gait is inherently unstable, and that a feedback control is thus necessary for stabilization. Although there are many criteria for the evaluation of a running gait, we evaluate

* Corresponding author. E-mail: fasano@jaist.ac.jp

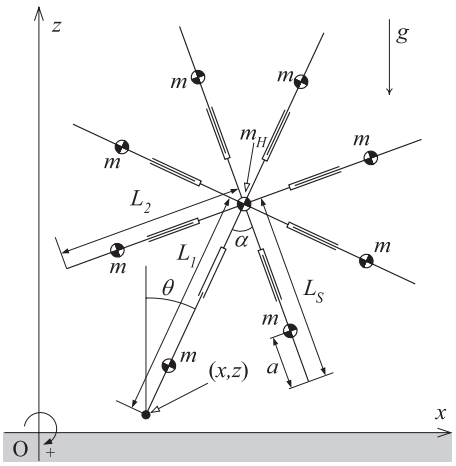

Fig. 1. Model of telescopic-legged rimless wheel.

it in terms of the walking speed and specific resistance, and compare the efficiency with that of the walking gait. The numerical analysis also shows that there is a gap between the stable domain of the walking gait and that of the running gait. We then investigate the potentiality of another type of locomotion in the gap aiming at the skipping which is known as a style of gait movement involving a combination of walking and jumping. The properties and mechanisms of skipping have been studied in various fields.[10,11] However, there are almost no studies on skipping in the field of robotics. We then numerically show that a stable skipping gait emerges by shortening the control period of the telescopic-legs' action, and compare the properties of the generated skipping gait with those of the other two gaits. Throughout the gait analysis, we classify the three gaits from the efficiency and inherent stability points of view.

This paper is organized as follows. In Section 2, we introduce the model of a planar telescopic-legged rimless wheel and design an output following control for the telescopic-legs' action. Generating a level walking gait is also described in this section. In Section 3, we numerically show that a stable running gait can be generated by employing a simple feedback control of the desired settling time, and compare the properties of the generated running gait with those of the walking gait. In Section 4, we numerically show that an inherently stable skipping gait can be generated without any additional control laws, and compare the properties of the generated skipping gait with those of the other two gaits. Section 5 concludes this paper and describes future research directions.

2. Modeling and Control

This section describes motion equations of the robot focusing on the phase sequence in the typical running gait because the walking motion can be easily derived from the running motion only by loss of the flight phase. Equations of the skipping gait are described in Section 4. At the end of this section, a typical walking gait is generated using the derived equations.

2.1. Robot model and its equations of motion

This paper deals with a planar telescopic-legged rimless wheel as shown in Fig. 1. This robot consists of eight identical telescopic legs whose mass is m [kg], and has a "hip" mass of m_H [kg] at the central position. Every leg has a control force for the telescopic-leg's actuation. We assume, however, that only two control forces: u_1 of the stance-leg and u_2 of the previous one, are available, and that other six legs are mechanically locked. Let $\boldsymbol{q} \in \mathbb{R}^5$ be the generalized coordinate vector defined as

$$\boldsymbol{q}^T = [x \quad z \quad \theta \quad L_1 \quad L_2]. \tag{1}$$

Here, (x, z) is the tip position of the stance leg, θ rad is the angular position of the stance leg with respect to vertical, and L_1 [m] and L_2 [m] are the lengths of the stance and previous-stance legs. We conduct precise numerical simulations by taking the contracting motion of the previous stance-leg into account. This robot can generate a stable and high-speed walking gait on level ground only by extending the stance leg during stance phases while contracting the previous stance-leg.[7] The primary purpose of this approach is to asymmetrize the impact posture to make overcoming the potential barrier at midstance easy. The mechanical energy is consequently restored. This approach is also effective in the bipedal case.[8]

We assume the following conditions.

- The collision of the next stance-leg with the ground is inelastic.
- The contact point of the stance leg with the ground does not slip or bounce during stance phases.
- The control of the telescopic legs is completed before next collisions. (Settling-time condition)
- The leg lengths except those of the stance and previous-stance legs are maintained the shortest length, L_s [m].

2.1.1. Stance phase. The robot's dynamic equation during stance phases becomes

$$\boldsymbol{M}(\boldsymbol{q})\ddot{\boldsymbol{q}} + \boldsymbol{h}(\boldsymbol{q}, \dot{\boldsymbol{q}}) = \boldsymbol{S}\boldsymbol{u} + \boldsymbol{J}^T\boldsymbol{\lambda}, \tag{2}$$

where $\boldsymbol{\lambda} \in \mathbb{R}^2$ is the Lagrange undetermined multiplier vector, and $\boldsymbol{S}\boldsymbol{u} \in \mathbb{R}^5$ is the control input vector which is detailed as

$$\boldsymbol{S}\boldsymbol{u} = \begin{bmatrix} 0 & 0 \\ 0 & 0 \\ 0 & 0 \\ 1 & 0 \\ 0 & 1 \end{bmatrix} \begin{bmatrix} u_1 \\ u_2 \end{bmatrix}. \tag{3}$$

The velocity conditions of the tip position of the stance leg are given by $\dot{x} = 0$, $\dot{z} = 0$, and these are then summarized as

$$\boldsymbol{J}\dot{\boldsymbol{q}} = \boldsymbol{0}_{2\times 1}, \quad \boldsymbol{J} := \begin{bmatrix} 1 & 0 & 0 & 0 & 0 \\ 0 & 1 & 0 & 0 & 0 \end{bmatrix}. \tag{4}$$

We can solve Eqs. (2) and (4) for $\boldsymbol{\lambda}$ as

$$\boldsymbol{\lambda} = -(\boldsymbol{J}\boldsymbol{M}(\boldsymbol{q})^{-1}\boldsymbol{J}^T)^{-1}\boldsymbol{J}\boldsymbol{M}(\boldsymbol{q})^{-1}(\boldsymbol{S}\boldsymbol{u} - \boldsymbol{h}(\boldsymbol{q}, \dot{\boldsymbol{q}})). \tag{5}$$

The first element of $\boldsymbol{\lambda} \in \mathbb{R}^2$ represents the horizontal ground reaction force and the second the vertical ground reaction force. We can detect the instant of take-off by observing the

https://doi.org/10.1017/S0263574711001226 Published online by Cambridge University Press

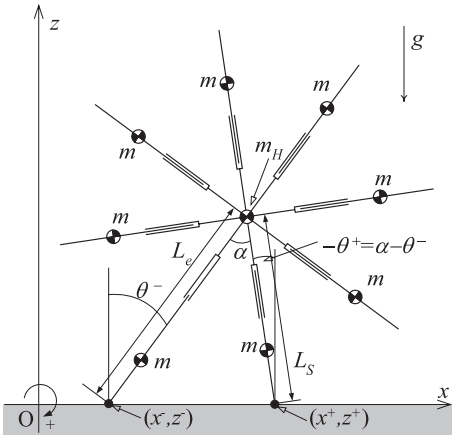

Fig. 2. Configuration at impact.

sign of the second element; the robot starts jumping when the value becomes zero.

2.1.2. Flight phase. During flight phases, the holonomic constraint force becomes zero and the dynamic equation becomes the same as Eq. (2) where $\boldsymbol{\lambda} = \mathbf{0}_{2\times 1}$.

2.1.3. Collision phase. As previously mentioned, we assumed that the control of the telescopic legs is completed before next collision, and that the next stance-leg length is kept L_s [m]. Figure 2 shows the configuration at impact. The stance leg is on the ground in the walking or skipping gaits as shown in this figure, whereas it is floating in the air in the running gait. The inelastic collision with the ground is modeled as

$$\boldsymbol{M}(\theta^-)\dot{\boldsymbol{q}}^+ = \boldsymbol{M}(\theta^-)\dot{\boldsymbol{q}}^- - \boldsymbol{J}_I(\theta^-)^T\boldsymbol{\lambda}_I, \tag{6}$$

$$\boldsymbol{J}_I(\theta^-)\dot{\boldsymbol{q}}^+ = \mathbf{0}_{4\times 1}. \tag{7}$$

In the following, the detail of $\boldsymbol{J}_I(\theta^-) \in \mathbb{R}^{4\times 5}$ is described. As shown in Fig. 2, (x^+, z^+) is the tip position of the stance leg just after impact and its time derivatives must be zero. The velocity constraint conditions are then specified as

$$\frac{\mathrm{d}}{\mathrm{d}t}(x^- + L_e\sin\theta^- + L_s\sin(\alpha-\theta^-)) = 0, \tag{8}$$

$$\frac{\mathrm{d}}{\mathrm{d}t}(z^- + L_e\cos\theta^- - L_s\cos(\alpha-\theta^-)) = 0, \tag{9}$$

where L_e [m] is the desired terminal length and $L_e > L_s$. These equations are arranged as

$$\dot{x}^+ + L_e\dot{\theta}^+\cos\theta^- - L_s\dot{\theta}^+\cos(\alpha-\theta^-) = 0, \tag{10}$$

$$\dot{z}^+ - L_e\dot{\theta}^+\sin\theta^- - L_s\dot{\theta}^+\sin(\alpha-\theta^-) = 0. \tag{11}$$

Here, note that $\dot{x}^+ \neq \frac{\mathrm{d}}{\mathrm{d}t}(x^+) = 0$ and $\dot{z}^+ \neq \frac{\mathrm{d}}{\mathrm{d}t}(z^+) = 0$ because (x, z) is not updated. $\dot{x}^+$ in Eq. (10) and $\dot{z}^+$ in Eq. (11) are the tip velocities just after impact of the previous stance leg. These are reset to zero after $\dot{\boldsymbol{q}}^+$ is derived. We also assume that the prismatic joints are mechanically locked at impact, i.e.,

$$\dot{L}_1^+ = 0, \tag{12}$$

$$\dot{L}_2^+ = 0. \tag{13}$$

$\boldsymbol{J}_I(\theta^-)$ is then formulated by summarizing the four conditions in Eqs. (10)–(13) as

$$\boldsymbol{J}_I(\theta^-) = \begin{bmatrix} 1 & 0 & L_e\cos\theta^- - L_s\cos(\alpha-\theta^-) & 0 & 0 \\ 0 & 1 & -L_e\sin\theta^- - L_s\sin(\alpha-\theta^-) & 0 & 0 \\ 0 & 0 & 0 & 1 & 0 \\ 0 & 0 & 0 & 0 & 1 \end{bmatrix}. \tag{14}$$

By solving Eqs. (6) and (7) for $\dot{\boldsymbol{q}}^+$, we get

$$\dot{\boldsymbol{q}}^+ = (\boldsymbol{I}_5 - \boldsymbol{M}(\theta^-)^{-1}\boldsymbol{J}_I(\theta^-)^T(\boldsymbol{J}_I(\theta^-)\boldsymbol{M}(\theta^-)^{-1} \boldsymbol{J}_I(\theta^-)^T)^{-1}\boldsymbol{J}_I(\theta^-))\dot{\boldsymbol{q}}^-. \tag{15}$$

Here, we must replace the first and the second elements of $\dot{\boldsymbol{q}}^+$ with zeros because $\dot{x}^+$ and $\dot{z}^+$ are the tip velocities of the previous stance leg and are not zeros as previously mentioned. Accordingly, the positional vector just after impact, $\boldsymbol{q}^+$, must be reset to

$$\boldsymbol{q}^+ = \begin{bmatrix} 0 \\ 0 \\ \theta^- - \alpha \\ L_s \\ L_e \end{bmatrix}. \tag{16}$$

2.2. Output following control for telescopic-leg motion

We choose L_1 and L_2 as the control outputs of the system. These can be written as

$$\boldsymbol{y} := \begin{bmatrix} L_1 \\ L_2 \end{bmatrix} = \boldsymbol{S}^T\boldsymbol{q}. \tag{17}$$

The second-order derivative of $\boldsymbol{y}$ with respect to time becomes

$$\ddot{\boldsymbol{y}} = \boldsymbol{S}^{\mathrm{T}}\boldsymbol{M}(\boldsymbol{q})^{-1}(\boldsymbol{S}\boldsymbol{u} - \boldsymbol{h}(\boldsymbol{q},\dot{\boldsymbol{q}}) - \boldsymbol{J}^T\boldsymbol{\lambda}), \tag{18}$$

where $\boldsymbol{\lambda}$ is of Eq. (5) or $\mathbf{0}_{2\times 1}$. During stance phases, by substituting Eq. (5) into Eq. (18) and arranging it, we obtain

$$\ddot{\boldsymbol{y}} = \boldsymbol{S}^T\boldsymbol{M}(\boldsymbol{q})^{-1}\boldsymbol{Y}(\boldsymbol{q})\left(\boldsymbol{S}\boldsymbol{u} - \boldsymbol{h}(\boldsymbol{q},\dot{\boldsymbol{q}})\right), \tag{19}$$

$$\boldsymbol{Y}(\boldsymbol{q}) := \boldsymbol{I}_5 - \boldsymbol{J}^T(\boldsymbol{J}\boldsymbol{M}(\boldsymbol{q})^{-1}\boldsymbol{J}^T)^{-1}\boldsymbol{J}\boldsymbol{M}(\boldsymbol{q})^{-1}. \tag{20}$$

Then, we can consider the following control input for achieving $\boldsymbol{y} \to \boldsymbol{y}_{\mathrm{d}}(t)$:

$$\boldsymbol{u} = \boldsymbol{A}(\boldsymbol{q})^{-1}(\boldsymbol{v} + \boldsymbol{B}(\boldsymbol{q},\dot{\boldsymbol{q}})), \tag{21}$$

$$\boldsymbol{v} = \ddot{\boldsymbol{y}}_{\mathrm{d}}(t) + \boldsymbol{K}_D(\dot{\boldsymbol{y}}_{\mathrm{d}}(t) - \dot{\boldsymbol{y}}) + \boldsymbol{K}_P(\boldsymbol{y}_{\mathrm{d}}(t) - \boldsymbol{y},) \tag{22}$$

where $\boldsymbol{K}_P \in \mathbb{R}^{2\times 2}$ and $\boldsymbol{K}_D \in \mathbb{R}^{2\times 2}$ are the PD-gain matrices and are positive diagonal matrices. $\boldsymbol{A}(\boldsymbol{q}) \in \mathbb{R}^{2\times 2}$ and

https://doi.org/10.1017/S0263574711001226 Published online by Cambridge University Press

$\boldsymbol{B}(\boldsymbol{q}, \dot{\boldsymbol{q}}) \in \mathbb{R}^2$ are defined as

$$\boldsymbol{A}(\boldsymbol{q}) := \boldsymbol{S}^T \boldsymbol{M}(\boldsymbol{q})^{-1} \boldsymbol{Y}(\boldsymbol{q}) \boldsymbol{S}, \tag{23}$$

$$\boldsymbol{B}(\boldsymbol{q}, \dot{\boldsymbol{q}}) := \boldsymbol{S}^T \boldsymbol{M}(\boldsymbol{q})^{-1} \boldsymbol{Y}(\boldsymbol{q}) \boldsymbol{h}(\boldsymbol{q}, \dot{\boldsymbol{q}}). \tag{24}$$

During flight phases, we can formulate the control input as the above equations by replacing matrix $\boldsymbol{Y}(\boldsymbol{q})$ with $\boldsymbol{I}_5$.

2.3. Desired-time trajectory

Here, we define the basic parameters, terms, and their notations used for specifying the output following control.

Definition 1 *Let t [s] be the time parameter. This is reset at every instant of the stance-leg exchange and is nonnegative.*

Definition 2 *Time interval T [s], which is the steady value of the interval from the instant of one stance-leg exchange to the next, is called the "step period."*

Definition 3 *The robot starts locomotion from an initial condition at* 0 *s; this is defined as the* 0th *collision. The next collision for stance-leg exchange is the* 1st *collision, and the motion between the* 0th and 1st collisions is called the "1st step." The subsequent collisions and steps are contextually counted.

Definition 4 *Let $T_{\rm set}$ [s] be the desired settling time for output following control of the two legs. We assume that $T \geq T_{\rm set}$ holds in a steady gait. This is called the "settling-time condition."*

The desired-time trajectories for smooth telescopic-legs' motion can be formulated as 5-order functions of time as follows:

$$L_{1\rm d}(t) = \begin{cases} a_5 t^5 + a_4 t^4 + a_3 t^3 + a_0, & (0 \leq t < T_{\rm set}), \\ L_e, & (t \geq T_{\rm set}), \end{cases} \tag{25}$$

$$L_{2\rm d}(t) = L_s + L_e - L_{1\rm d}(t). \tag{26}$$

The boundary conditions are given by $L_{1\rm d}(0^+) = L_s$, $\dot{L}_{1\rm d}(0^+) = 0$, $\ddot{L}_{1\rm d}(0^+) = 0$, $L_{1\rm d}(T_{\rm set}) = L_e$, $\dot{L}_{1\rm d}(T_{\rm set}) = 0$, and $\ddot{L}_{1\rm d}(T_{\rm set}) = 0$. The coefficients a_5, a_4, a_3 and a_0 are then determined as

$$a_5 = \frac{6(L_e - L_s)}{T_{\rm set}^5}, \quad a_4 = -\frac{15(L_e - L_s)}{T_{\rm set}^4},$$
$$a_3 = \frac{10(L_e - L_s)}{T_{\rm set}^3}, \quad a_0 = L_s.$$

2.4. Walking gait generation

Since the detailed analysis of the walking gait has already been reported in refs. [6–8], here we'd like to simply observe the typical motion.

Figure 3 shows the simulation results of a steady walking gait, where $T_{\rm set} = 0.40$ s. Here, (a) shows the lengths of the telescopic legs, (b) the angular position, and (c) the vertical ground reaction force. The physical and control parameters were chosen as listed in Table I. The leg mass, m, was chosen sufficiently smaller than the hip mass, m_H, so that the contracting motion of the previous stance leg does not affect the motion. Figure 4 shows the stick diagram for the three steady steps, and we can confirm that the impact posture is successfully tilted forward by the control. Figure 3(b) shows that the angular position just after impact, θ^+, is negative and the potential barrier thus remains. As discussed in ref. [8], the potential barrier is necessary for controlling the excessive forward acceleration and functions as a brake. Figure 3(c) shows that there exist indifferentiable points during stance phases. This instant is equal to $T_{\rm set}$ [s], and the robot begins to fall down as a 1-DOF rigid body.

Table I. Parameter settings.

m_H	10.0	kg			
m	0.10	kg	α	$\pi/4$	rad
a	0.30	m	$\boldsymbol{K}_D$	$100\boldsymbol{I}_2$	
L_s	1.00	m	$\boldsymbol{K}_P$	$2500\boldsymbol{I}_2$	
L_e	1.15	m			

The authors investigated the properties of the generated walking gait and the effects of forefeet on the efficiency in detail. Here are the main results reported in refs. [6–8].

- The gait efficiency is monotonically improved as the impact posture is more asymmetrized.
- The problems are that the vertical ground reaction force becomes negative or the robot begins to jump, and that the time margin of the control period reaches the limit as the walking speed increases.
- The geometric effect of the attached forefeet significantly promotes asymmetrizing the impact posture, and the efficiency of the generated walking gait is dramatically improved. Also, the effect monotonically increases as the foot length increases.
- A biped robot with telescopic legs can also generate high-speed level gaits by asymmetrizing the impact posture. Adding elastic elements to the ankle joints for the purpose of braking is effective for increasing the time margin of the control period. The zero moment point often reaches to the tiptoe in return for the braking, and a tiptoe motion (forefoot weight-bearing) would emerge.

3. Running Gait Generation

3.1. Intuitive feedback control laws for stabilization

3.1.1. Control of desired settling time. We first try to generate a stable running gait. Since there are many control parameters, we chose and fixed the main parameters as listed in Table I. We then adjust the desired settling time, $T_{\rm set}$.

As described later, it is impossible to generate a stable running gait only by adjusting $T_{\rm set}$ because the motion is inherently unstable. We then propose a heuristic control of the desired settling time for stabilization. Let $i \geq 0$ be the step number, and consider the following control:

$$T_{\rm set}[i+1] = T_{\rm set}^* - \zeta(T[i] - T^*), \tag{27}$$

where $i \geq 1$, $\zeta > 0$ is the feedback gain, and $T_{\rm set}^*$ [s] and T^* [s] are the target values of $T_{\rm set}$ and T. This control is based on the tendency that the step period increases from T^* if $T_{\rm set} > T_{\rm set}^*$ and decreases from T^* if $T_{\rm set} < T_{\rm set}^*$. Although $T_{\rm set}[i]$ and $T[i]$ do not converge to their target values, this control is very effective for stabilization to a 1-period running gait.

https://doi.org/10.1017/S0263574711001226 Published online by Cambridge University Press

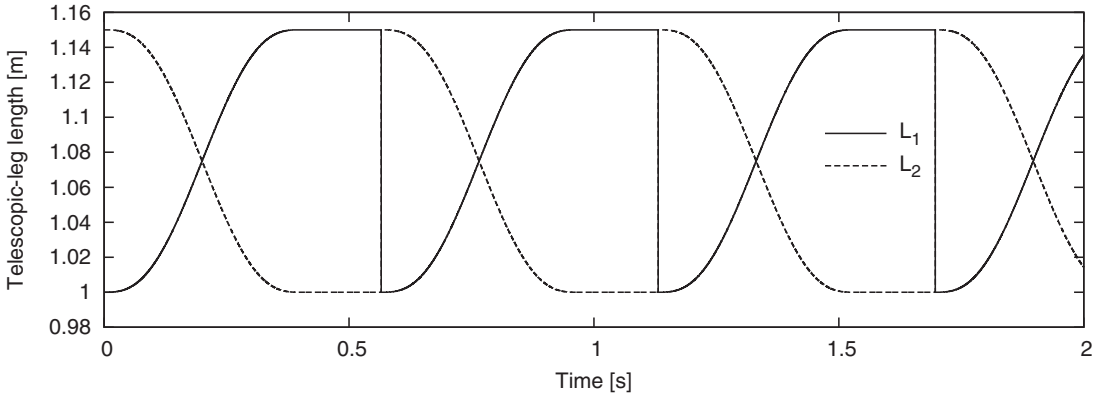

(a) Telescopic-leg length

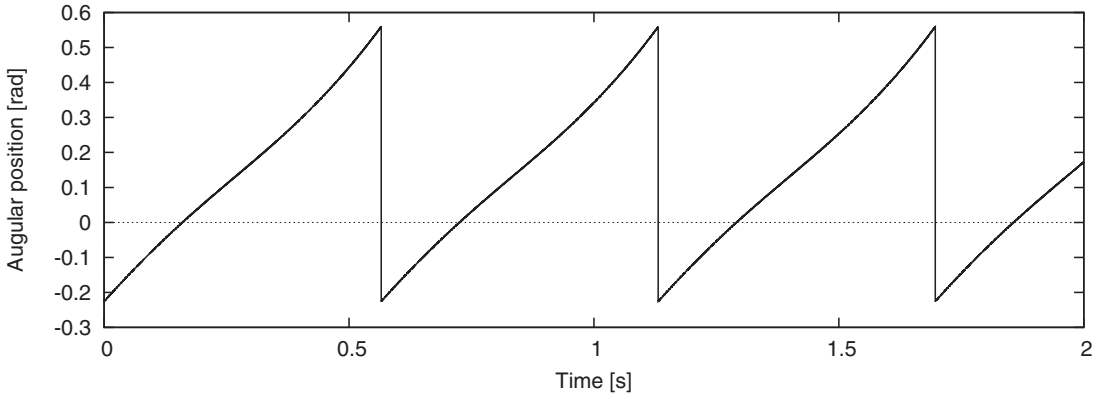

(b) Angular position

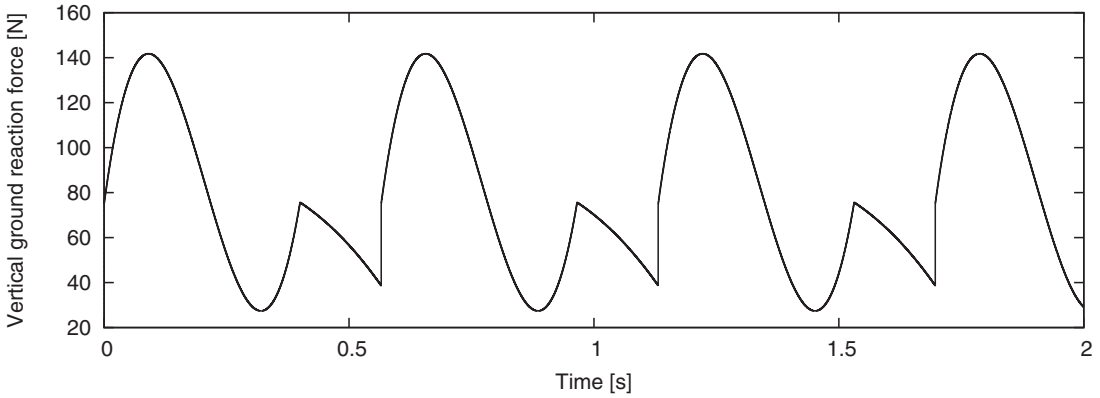

(c) Vertical ground reaction force

Fig. 3. Simulation results of steady walking. (a) Telescopic-leg length; (b) angular position; (c) vertical ground reaction force.

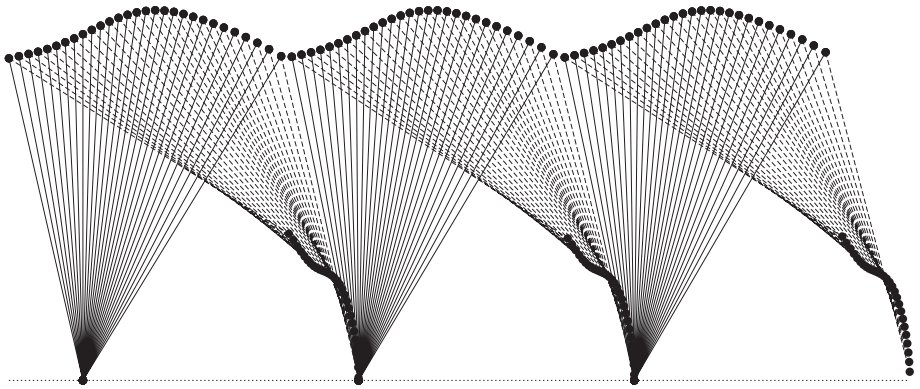

Fig. 4. Stick diagram for steady walking gait.

https://doi.org/10.1017/S0263574711001226 Published online by Cambridge University Press

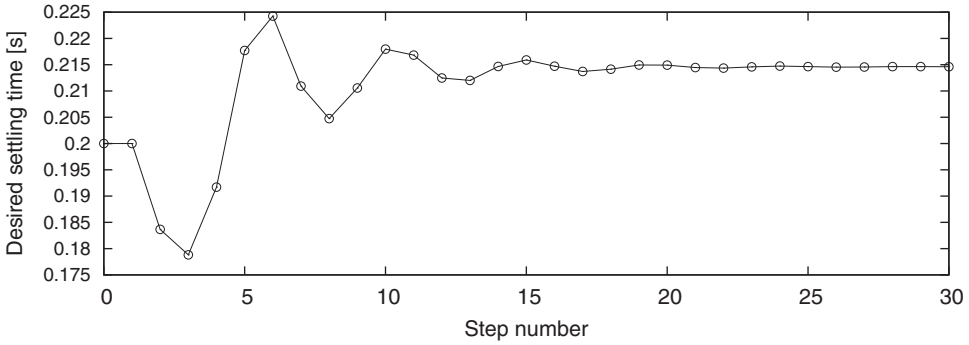

(a) Desired settling time

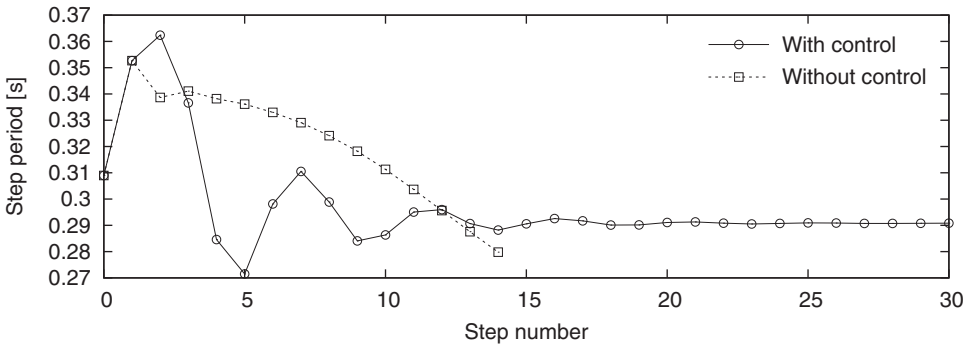

(b) Step period

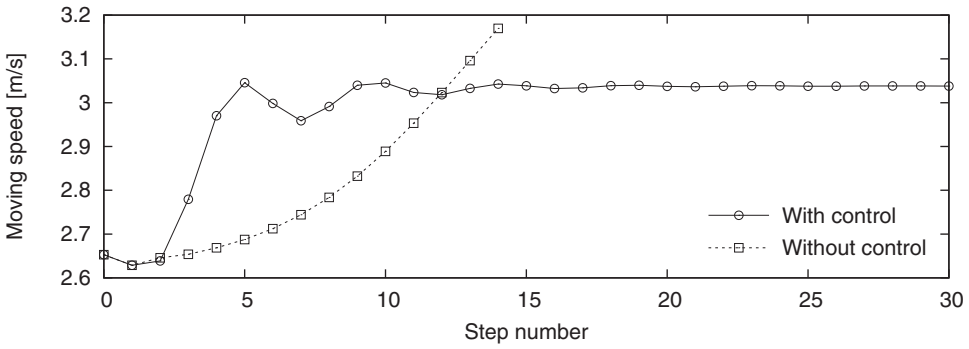

(c) Moving speed

Fig. 5. Convergence of gait descriptors. (a) Desired settling time; (b) Step period; (c) Moving speed.

The desired trajectories are accordingly updated as follows. Let a_{ji} ($j = 0, 3, 4, 5$) be the coefficient of the desired trajectory for $L_{1\mathrm{d}}(t)$ corresponding to a_j in Eq. (25), and they are recalculated at ith impact of the stance-leg exchange as

$$a_{5i} = \frac{6(L_e - L_s)}{T_{\mathrm{set}}[i]^5}, \quad a_{4i} = -\frac{15(L_e - L_s)}{T_{\mathrm{set}}[i]^4},$$
$$a_{3i} = \frac{10(L_e - L_s)}{T_{\mathrm{set}}[i]^3}, \quad a_{0i} = L_s.$$

The desired trajectories for the ith step are accordingly determined as follows:

$$L_{1\mathrm{d}}^{(i)}(t) = \begin{cases} a_{5i}t^5 + a_{4i}t^4 + a_{3i}t^3 + a_{0i}, & (0 \le t < T_{\mathrm{set}}[i]), \\ L_e, & (t \ge T_{\mathrm{set}}[i]), \end{cases} \tag{28}$$

$$L_{2\mathrm{d}}^{(i)}(t) = L_s + L_e - L_{1\mathrm{d}}^{(i)}(t). \tag{29}$$

Figure 5 plots the evolutions of (a) the desired settling time, (b) the step period, and (c) the running speed with respect to the step number. Again, the basic parameters were chosen as listed in Table I, and the parameters for adjustment of T_{set} were chosen as $\zeta = 0.50$, $T^* = 0.320\,\mathrm{s}$ and $T^*_{\mathrm{set}} = 0.20\,\mathrm{s}$. The initial value of T_{set} was also chosen as $T_{\mathrm{set}}[0] = 0.20\,\mathrm{s}$. From the results, we can see that, although the convergence performance is not good, a stable gait is successfully generated in the case with the proposed feedback control. It should also be noted that, as described later, the running speed is more than twice the walking speed. In the case without the feedback control, although the motion is close to the limit cycle, the motion slowly diverges due to the instability aspect.

Figure 6 shows the simulation results of the steady running gait following the above simulation. Here, (a) is the lengths of the telescopic legs, (b) the angular position of the stance leg, and (c) the vertical reaction force. We can see that L_1 (L_2) is successfully controlled from L_s (L_e) to L_e (L_s) during the stance and flight phases. The angular position of the stance

https://doi.org/10.1017/S0263574711001226 Published online by Cambridge University Press

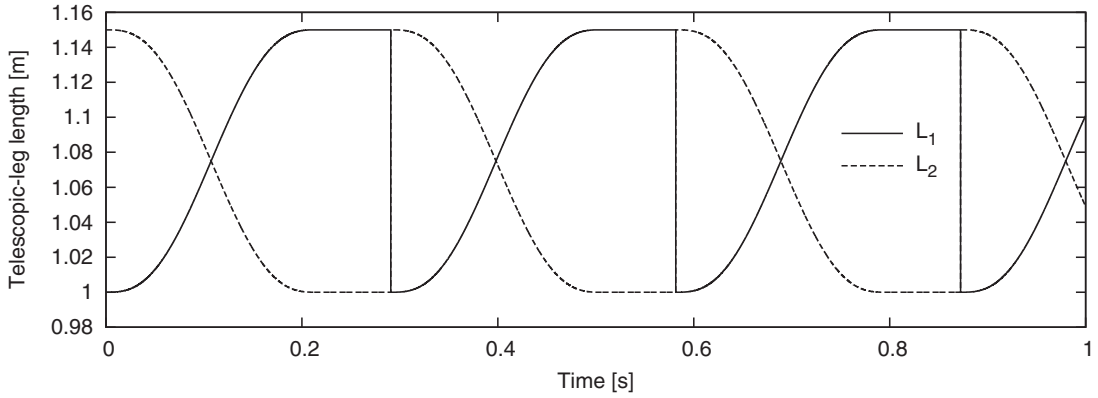

(a) Telescopic-leg length

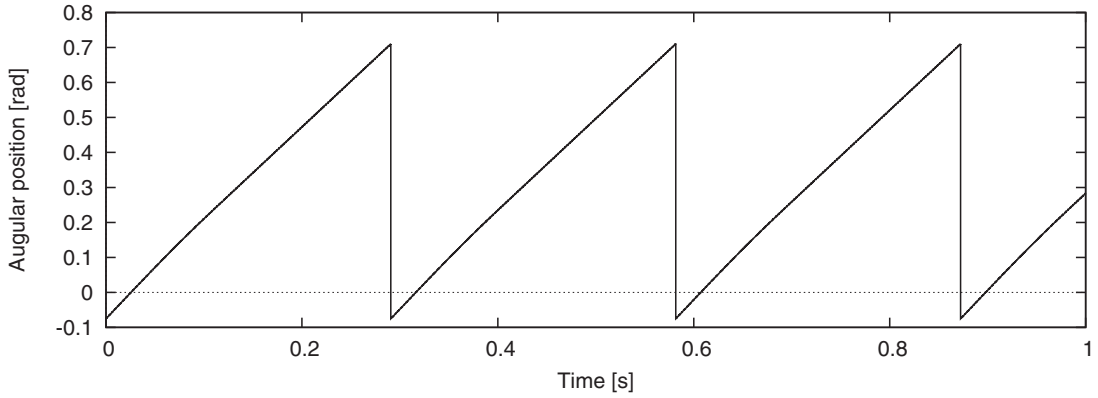

(b) Angular position

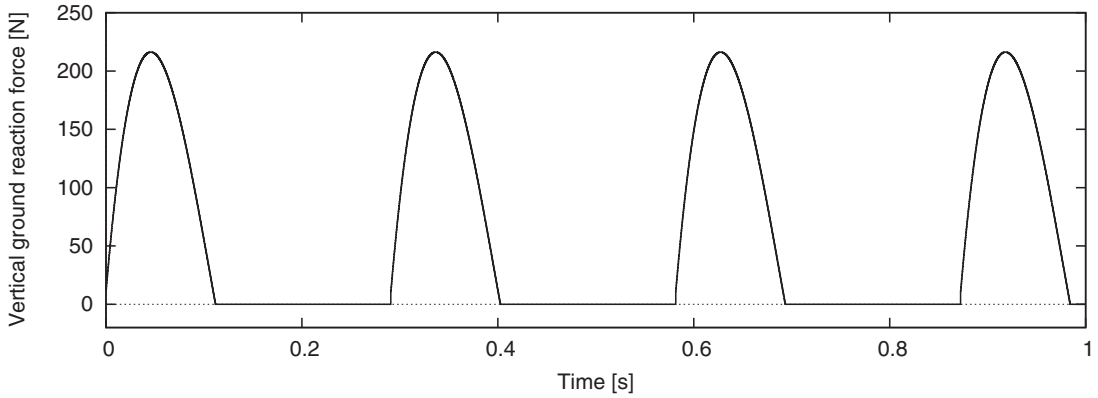

(c) Vertical ground reaction force

Fig. 6. Simulation results of steady running. (a) Telescopic-leg length; (b) angular position; (c) vertical ground reaction force.

leg just after impact is negative, and this implies that the impact posture is not sufficient for overcoming the potential barrier. This property is common to the walking and running gaits generated by the proposed output following control. Figure 7 plots the stick diagram of the stance and next stance legs. We can see that the flight phases emerge and the impact postures are more tilted forward.

3.1.2. Control of desired terminal length. The desired terminal length of the stance leg, L_e, can be considered to be another candidate of the parameter for stabilization. There is a tendency that the step period increases with the increase of L_e around the unstable equilibrium point. Let us then consider the following feedback control:

$$L_e[i+1] = L_e^* + \zeta(T[i] - T^*), \tag{30}$$

where L_e^* is the target value of L_e and is constant. This control is based on a tendency that the step period decreases from T^* if $L_e > L_e^*$ and increases from T^* if $L_e < L_e^*$.

In this case, the desired trajectories are updated at ith impact as follows:

$$L_{1\mathrm{d}}^{(i)}(t) = \begin{cases} a_{5i}t^5 + a_{4i}t^4 + a_{3i}t^3 + a_{0i}, & (0 \le t < T_{\mathrm{set}}), \\ L_e[i], & (t \ge T_{\mathrm{set}}), \end{cases} \tag{31}$$

https://doi.org/10.1017/S0263574711001226 Published online by Cambridge University Press

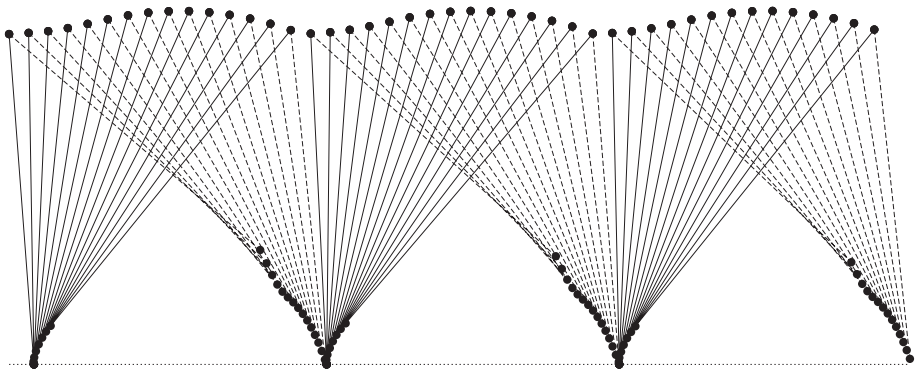

Fig. 7. Stick diagram for steady running gait.

$$L_{2\mathrm{d}}^{(i)}(t) = \begin{cases} L_s + L_e[i-1] - L_{1\mathrm{d}}^{(i-1)}(t), & (0 \le t < T_{\mathrm{set}}), \\ L_s, & (t \ge T_{\mathrm{set}}). \end{cases} \tag{32}$$

Here, note that $L_2(0^+) = L_e[i-1]$ and it is then smoothly controlled to L_s. The coefficients for the 5-order time-dependent function: a_5, a_4, a_3, and a_0, are accordingly updated at every instant of the stance-leg exchange as follows:

$$a_{5i} = \frac{6(L_e[i] - L_s)}{T_{\mathrm{set}}^5}, \quad a_{4i} = -\frac{15(L_e[i] - L_s)}{T_{\mathrm{set}}^4},$$
$$a_{3i} = \frac{10(L_e[i] - L_s)}{T_{\mathrm{set}}^3}, \quad a_{0i} = L_s.$$

Figure 8 plots the evolutions of (a) the desired terminal length, (b) the step period, and (c) the running speed with respect to the step number. Again, the basic parameters were chosen as listed in Table I except L_e. The parameters for adjustment of L_e were chosen as $\zeta = 0.35$, $T_{\mathrm{set}} = 0.20$ s, $T^* = 0.340$ s, and $L_e^* = 1.15$ s. The initial value of L_e was also chosen as $L_e[0] = 1.15$ s. We can see that the generated gait converges to a stable 1-period limit cycle while updating L_e.

This approach has also been shown to be effective. In the following, however, we'd like to use the feedback control of T_{set} only for stabilization to systematically evaluate the properties of the walking, running, and skipping gaits under the same rolling radius.

3.2. *Efficiency analysis*

3.2.1. Walking speed and specific resistance. We analyze the efficiency of the generated running gait by changing the target step period, T^*. In this case, the desired settling time, T_{set}, cannot be systematically changed. Figure 9 plots the moving speed as a function of T_{set}. Since the leg mass is sufficiently small compared to the hip mass, the moving speed was approximately calculated by dividing the travel distance of the central position of the body frame, i.e., the position of m_H, by the step period. We can see that the speed of the generated gaits is very fast and almost monotonically increases with the increase of T_{set}. As seen from the enlarged view, however, the moving speed is not uniquely determined with respect to T_{set}. This suggests that two different gaits can be generated in accordance with the system parameters.

The energy efficiency of limit-cycle runners can be evaluated in terms of specific resistance (SR) which is defined as

$$\mathrm{SR} := \frac{p}{Mgv}, \tag{33}$$

where $M := m_H + 8m$ [kg] is the robot's total mass and p [J/s] is the average input power which is defined as

$$p := \frac{1}{T}\int_{0^+}^{T_{\mathrm{set}}} (|\dot{L}_1 u_1| + |\dot{L}_2 u_2|)\,\mathrm{d}t. \tag{34}$$

Here, SR expresses the consumed energy per unit mass and per unit length traveled, and is a dimensionless quantity. The smaller its value, the better the energy efficiency. Note that the real robot consumes energy not only by actuating the telescopic legs but also by maintaining the lengths of the other six legs during motion. We assumed that the other six legs are mechanically locked and they do not need any energy supply.

Figure 10 plots the moving speed versus the SR. We can see that there are one-to-one relationships between the moving speed and specific resistance. It should be noted that the faster the moving speed, the better the energy efficiency. This implies that the change in the consumed energy is much flatter than that in the moving speed.

3.2.2. Walking versus running. Here, we compare the properties of the generated running gait with those of the walking gait. Figure 11 plots the moving speeds as the functions of T_{set}. We also generated the walking gaits by using the same model and parameters by changing T_{set}. The result strongly supports that the running gaits achieve much faster than the walking gaits. The moving speed in the running gait is very sensitive to T_{set}, whereas there is little change in the walking gait although the range of T_{set} is wide.

Figure 12 shows the comparison of the SR. In virtual gravity approaches, the minimum SR yields $\tan\phi$ [-], where ϕ rad is the virtual slope. As one of the authors showed in ref. [12], a compass-like biped robot with semicircular feet achieves highly efficient limit-cycle walking with an SR of 0.01 [-] where $\phi = 0.01$ rad. Compared with this, we must conclude that the generated walking gaits are highly

https://doi.org/10.1017/S0263574711001226 Published online by Cambridge University Press

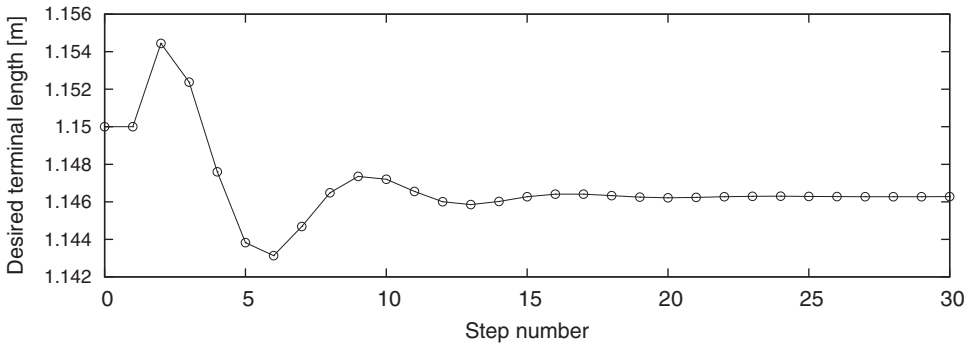

(a) Desired terminal length

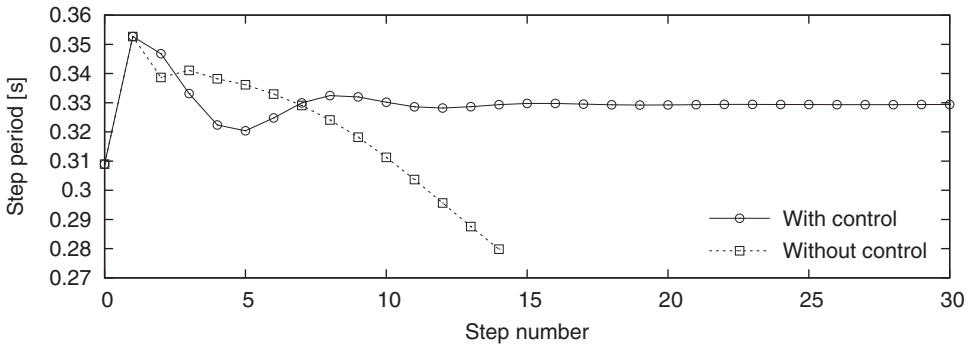

(b) Step period

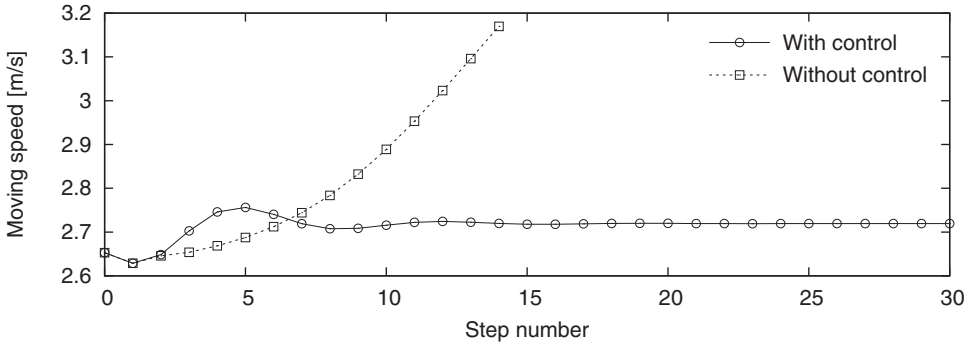

(c) Moving speed

Fig. 8. Convergence of gait descriptors. (a) Desired terminal length; (b) step period; (c) moving speed.

inefficient. In addition, the SR in the running gait is very sensitive to T_{set}, whereas there is little change in the walking gait. It should be noted that the energy efficiency in the running gait can be improved much better than that in the walking gait by suitably choosing T_{set}.

Note that there is a gap between the running domain and the walking one. There is a potentiality, however, that different gaits would emerge in the blank area by modifying the condition for detection of collision in the numerical simulator. Let us investigate this in the next section.

4. Skipping Gait Generation

4.1. Assumptions

This section investigates the potentiality and properties of limit-cycle skipping by using the same robot model and control law.

Skipping gaits involve another collision of the stance leg with the ground at the middle of the stance phase, which is then divided into the following five phases, as shown in Fig. 13.

(1) Stance phase I
The robot equations of motion during this phase are the same as those of the walking gait: Eqs. (2) and (4).

(2) Flight phase
As described in Section 2.1.2, the robot begins to flight when the vertical ground reaction force achieves zero from positive. The robot equation of motion during this phase is the same as Eq. (2), where $\boldsymbol{\lambda} = \mathbf{0}_{2\times 1}$.

(3) Collision phase I
The first collision of the stance leg with the ground occurs when $z = 0$. The conditions for the velocity constraint at this phase are given by $\dot{x}^+ = 0$ and $\dot{z}^+ = 0$. We should note, however, that the stance leg will begin to shrink due to the impact force if this collision occurs

https://doi.org/10.1017/S0263574711001226 Published online by Cambridge University Press

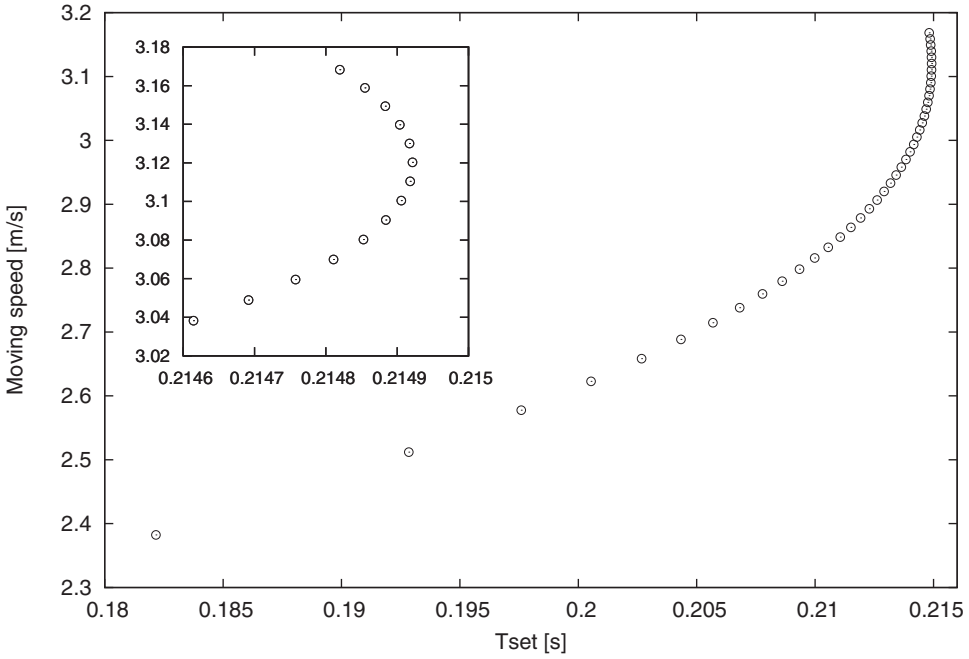

Fig. 9. Moving speed as a function of T_{set}.

in the middle of the output following control. We then derive the inelastic collision models depending on the settling-time condition.

The inelastic collision in this case is modeled as

$$\boldsymbol{M}(\boldsymbol{q}_s)\dot{\boldsymbol{q}}_s^+ = \boldsymbol{M}(\boldsymbol{q}_s)\dot{\boldsymbol{q}}_s^- - \boldsymbol{J}_s^T\boldsymbol{\lambda}_s, \tag{35}$$

where $\boldsymbol{J}_s$ is the Jacobian matrix derived depending on the settling-time condition. The size of $\boldsymbol{J}_s$ is not unique. Let T_s [s] be the time of this collision. We assume that the telescopic legs are mechanically locked in the case of $T_s \geq T_{\text{set}}$, i.e., the settling-time condition is met. The conditions of $\dot{L}_1^+ = 0$ and $\dot{L}_2^+ = 0$ are then added, and $\boldsymbol{J}_s$ in Eq. (35) becomes

$$\boldsymbol{J}_s = \begin{bmatrix} 1 & 0 & 0 & 0 & 0 \\ 0 & 1 & 0 & 0 & 0 \\ 0 & 0 & 0 & 1 & 0 \\ 0 & 0 & 0 & 0 & 1 \end{bmatrix}, \tag{36}$$

which should satisfy

$$\boldsymbol{J}_s\dot{\boldsymbol{q}}_s^+ = \boldsymbol{0}_{4\times 1}. \tag{37}$$

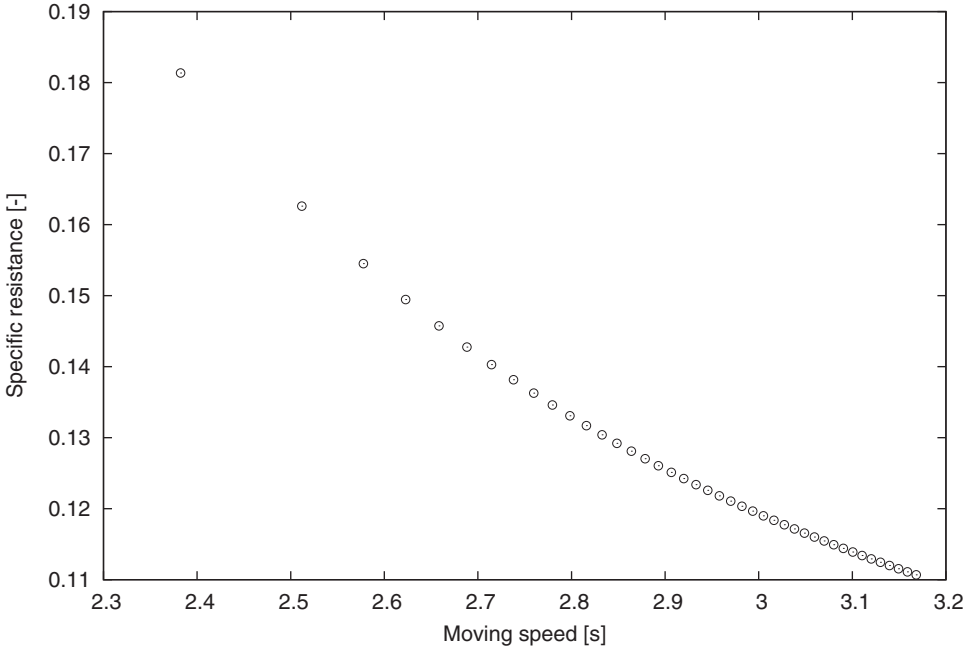

Fig. 10. Moving speed versus specific resistance.

https://doi.org/10.1017/S0263574711001226 Published online by Cambridge University Press

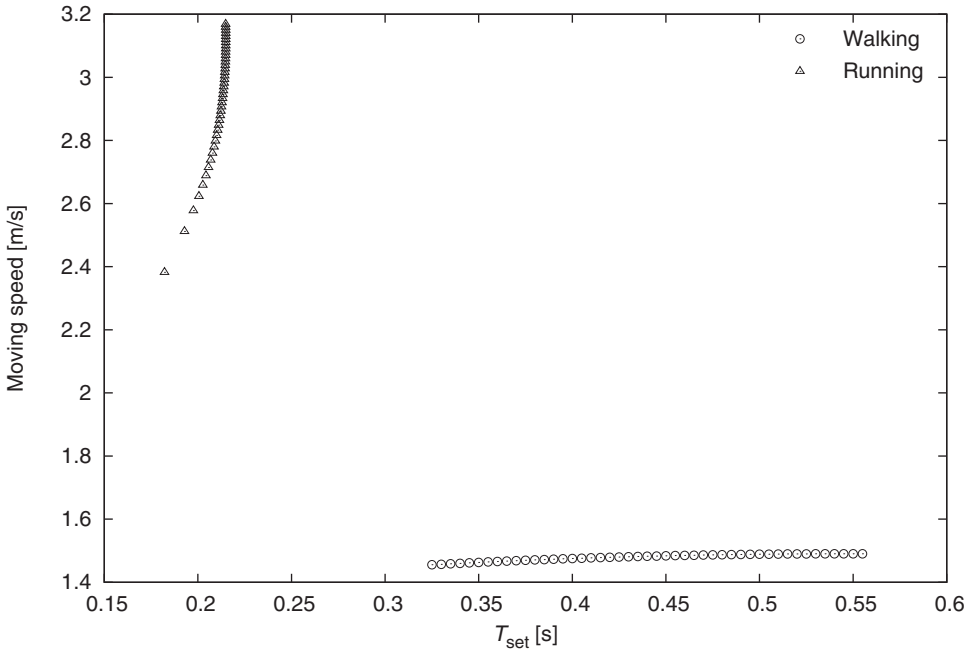

Fig. 11. Comparison of moving speeds as functions of T_{set}.

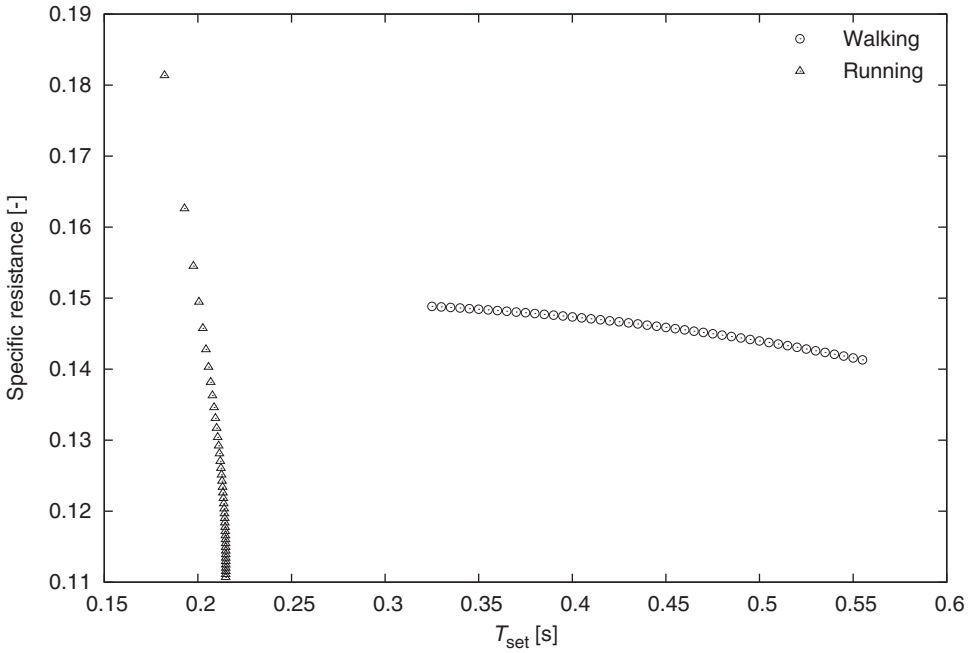

Fig. 12. Comparison of specific resistances as functions of T_{set}.

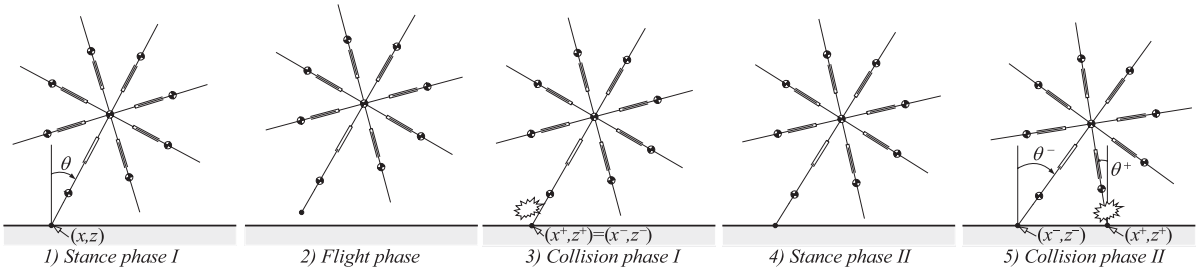

Fig. 13. Phase sequence in skipping gait.

https://doi.org/10.1017/S0263574711001226 Published online by Cambridge University Press

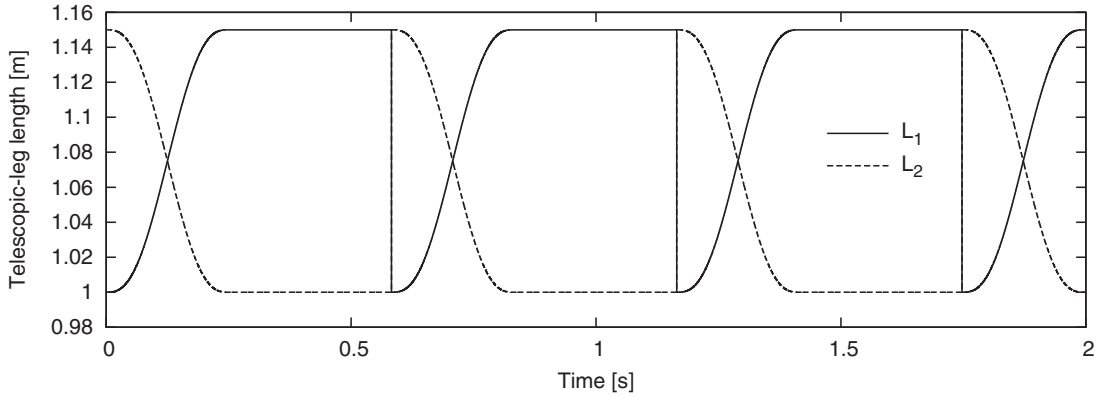

(a) Telescopic-leg length

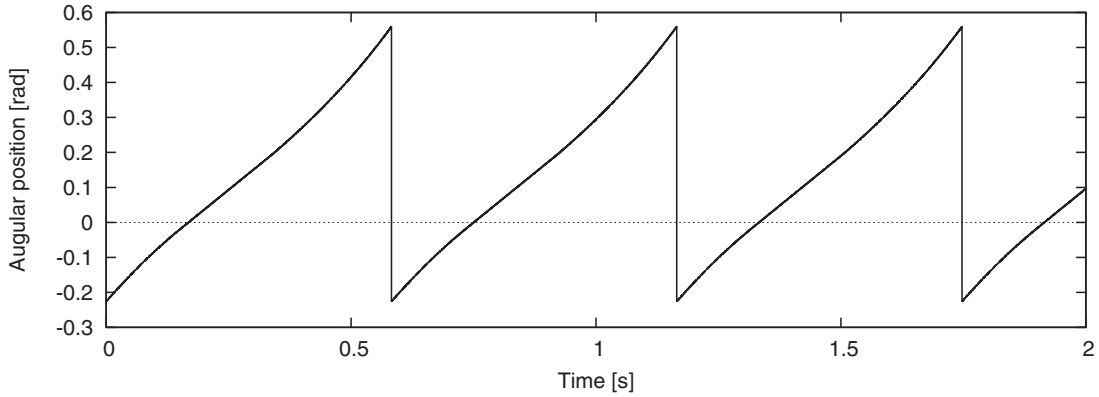

(b) Angular position

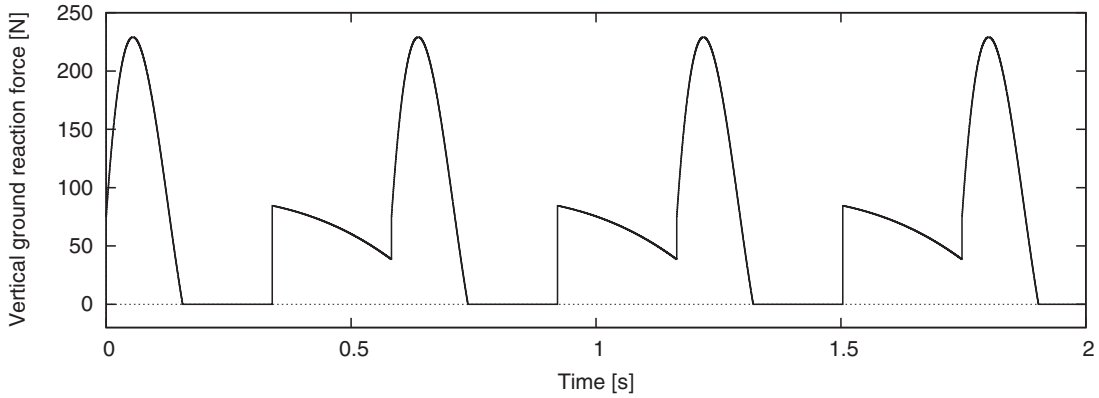

(c) Vertical ground reaction force

Fig. 14. Simulation results of skipping. (a) Telescopic-leg length; (b) angular position; (c) vertical ground reaction force.

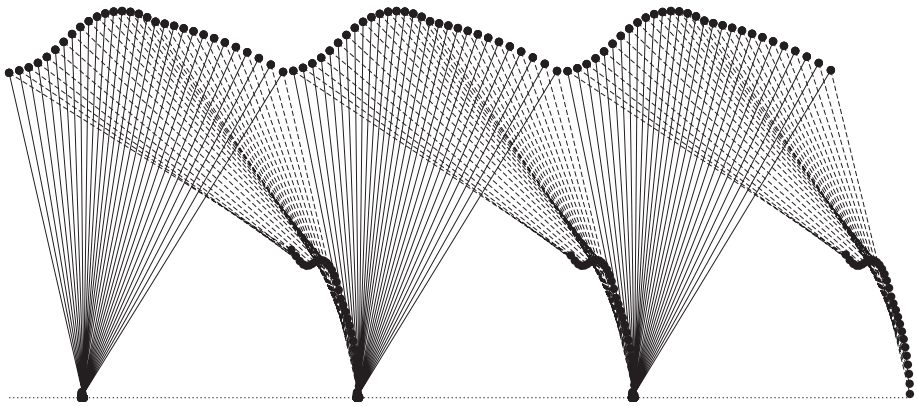

Fig. 15. Stick diagram for steady skipping gait.

https://doi.org/10.1017/S0263574711001226 Published online by Cambridge University Press

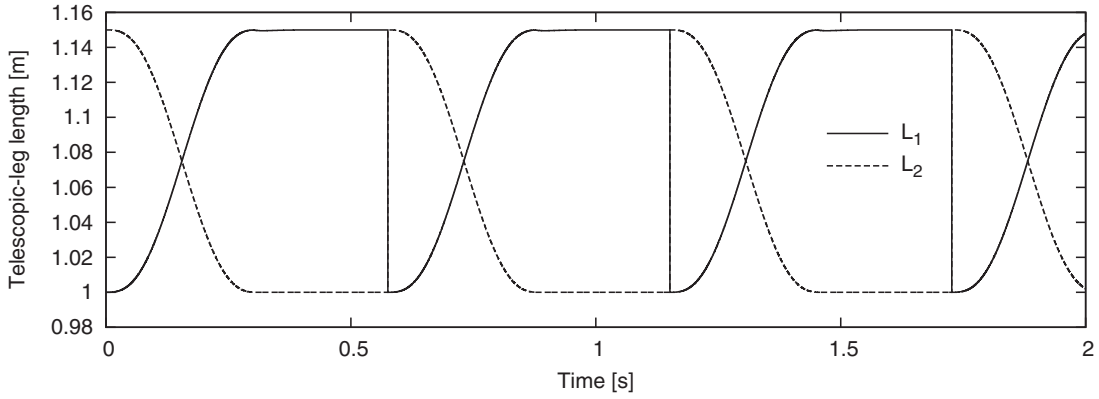

(a) Telescopic-leg length

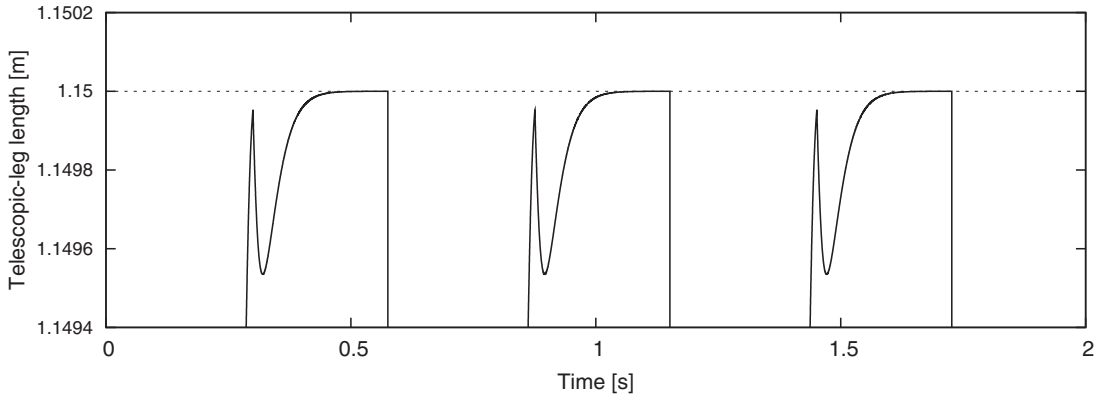

(b) Magnified view of (a)

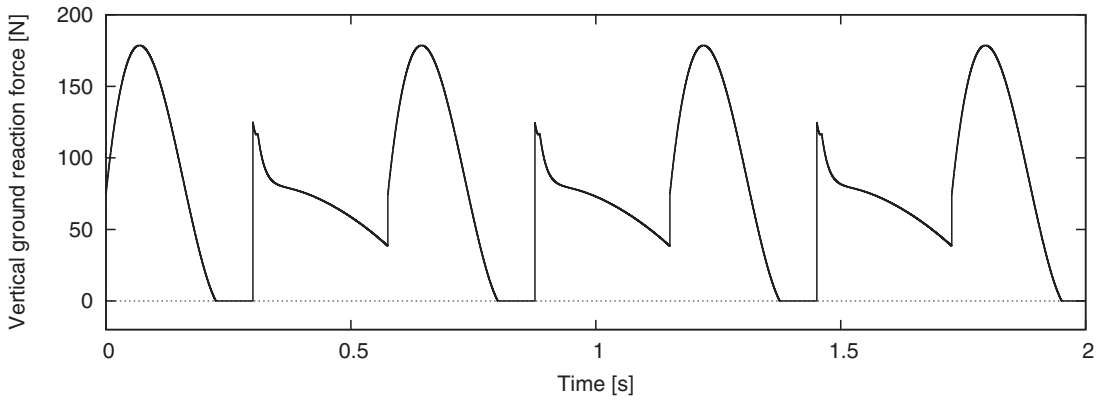

(c) Vertical ground reaction force

Fig. 16. Simulation results of skipping. (a) Telescopic-leg length; (b) magnified view of (a); (c) vertical ground reaction force.

Whereas in the case of $T_s < T_{\text{set}}$, we assume that the telescopic legs keep driving and are not mechanically locked. $\boldsymbol{J}_s$ in Eq. (35) then becomes

$$\boldsymbol{J}_s = \begin{bmatrix} 1 & 0 & 0 & 0 & 0 \\ 0 & 1 & 0 & 0 & 0 \end{bmatrix}, \tag{38}$$

which should satisfy

$$\boldsymbol{J}_s \dot{\boldsymbol{q}}_s^+ = \boldsymbol{0}_{2\times 1}. \tag{39}$$

By the effect of the output following control, however, the lengths of the telescopic legs are controlled to L_e and L_s again for a short time.

(4) Stance phase II
All equations are the same as those of stance phase I.

(5) Collision phase II (Stance-leg exchange)
The second collision occurs when the next stance leg hits the ground. All equations for the inelastic collision model are the same as those of the walking gait in Section 2.1.3: Eqs. (6) and (7).

4.2. Typical gait

We first try to generate a stable skipping gait. Unlike running, a skipping gait emerges only by conducting the output following control with a suitable settling of T_{set}. Figure 14 shows the simulation results of the steady skipping gait where $T_{\text{set}} = 0.25$ s. Here, (a) represents the lengths of the

https://doi.org/10.1017/S0263574711001226 Published online by Cambridge University Press

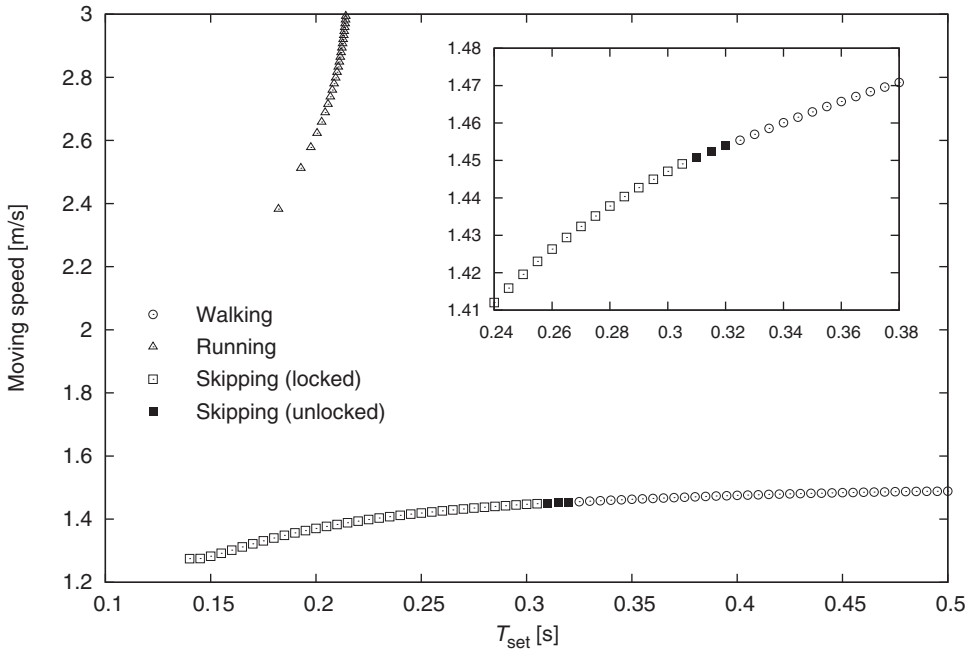

Fig. 17. Moving speeds as function of T_{set}.

telescopic-legs, (b) the angular position, and (c) the vertical ground reaction force. Figure 15 shows the stick diagram for the three steady steps. Again, the physical parameters were chosen as the same as those in the previous sections. In this case, the first collision of the stance leg with the ground (collision phase I) occurs more than 0.20 s after the stance-leg exchange (collision phase II). Therefore, the telescopic legs are mechanically locked and the robot lands on the ground as a 1-DOF rigid body. We can see that a skipping gait is successfully generated in accordance with the phase sequence of Fig. 13.

Figure 16 shows the simulation results of the steady skipping gait where $T_{set} = 0.31$ s. Here, (a) represents the lengths of the telescopic legs, (b) the magnified view of L_1 in (a), and (c) the vertical ground reaction force. In this case, the first collision of the stance leg occurs in the middle of the output following control, i.e. $T_s < T_{set}$, and the telescopic legs are thus unlocked at the instant. From (b), we can see that the stance leg immediately begins to start shrinking just after impact but it returns to $L_e = 1.15$ m before the next impact. Although we omit the details, the previous stance leg also a bit overshoots the nominal length, $L_s = 1.0$ m, due to the effect of the impact force but it returns to L_s soon. (c) also shows that the time change of vertical ground reaction force is similar to that of Fig. 14 (c) but it is affected by the control force of the stance leg, u_1, for pushing back just after the first collision.

4.3. Efficiency analysis

We evaluate the gait efficiency in terms of the walking speed and SR. Figure 17 plots the moving speeds of the three different gaits as functions of T_{set}. We can see that the skipping gaits emerge as an extension of the walking gaits, and that the moving speed monotonically decreases with the decrease of T_{set}. In addition, the skipping gaits unlocked at the collision phase I emerge near the boundary with the walking gait.

Figure 18 plots the SR of the three different gaits as functions of T_{set}. We can see that the SR in the walking and skipping gaits monotonically increases with the decrease of T_{set} and worsens more rapidly after the gait transition. From the magnified view, we can also see that the increasing tendency of the SR with respect to the decrease of T_{set} in the unlocked case is more rapid than that in the locked case. This is caused by the additional control force needed for extending the stance leg after shrinking due to the first collision.

We must conclude that the efficiency of the skipping gaits is the worst. Homogeneity of the walking and skipping gaits, however, creates an understanding that the stable domain of limit-cycle walking is dramatically extended by considering the condition of limit-cycle skipping.

Note that the range of T_{set} (stable domain) of the skipping gait overlaps with that of the running gait. Note also that, as previously described, the stable running gaits could not be generated without the feedback control of T_{set}. These imply that the running gait is different in properties from the other two gaits. Two factors make the difference. One is the initial angular velocity. A skipping gait can also be generated with the feedback control of T_{set} if the robot starts from a slower angular velocity. If we set the initial angular velocity to a sufficiently fast one, the gait converges to a stable running gait of the same T_{set}. The other is the inherent stability. Limit cycle gaits that are inherently stable naturally emerge under the suitable parameter settings, whereas those that are inherently unstable need specialized control techniques for stabilization. If the three different gaits can be dealt with from a unified standpoint, the design of a controller for adaptation to diverse situations would be formulated. More investigations are necessary.

5. Conclusion and Future Work

In this paper, we investigated the properties of the walking, running, and skipping gaits of the telescopic-legged rimless

https://doi.org/10.1017/S0263574711001226 Published online by Cambridge University Press

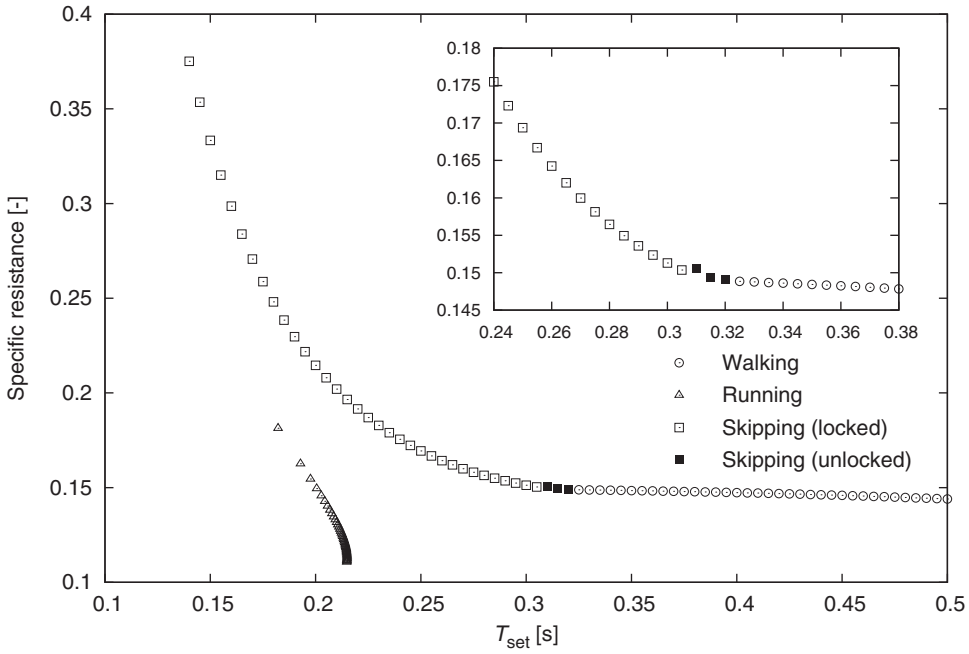

Fig. 18. Specific resistances as function of T_{set}.

wheel. It was shown that the proposed method based on robot's forward-tilting impact posture can also be used for generating the other two gaits only by adjustment of the desired settling time. Through the detailed gait analysis, we have learned two important features. One is that the generated walking and skipping gaits are inherently stable but the running gait is unstable only with the output following control. The other is that, by considering skipping, the stable domain of the walking gait is dramatically extended but the gait efficiency grows worse in terms of the moving speed and SR.

It would be expected that more various and adaptive gaits are generated by applying a unified controller taking the three gaits' properties into account. For this achievement, it is necessary to deeply understand the difference in stability between the running gait and the other two gaits. Improved design of limit-cycle runners is also left as an important subject to be investigated. There is a probability of making the running gait inherently stable and more energy-efficient by appropriately modifying the robot's body shape and mechanisms. Incorporating springs is a solution candidate for improving the energy-efficiency. Equivalent control laws using passive compliance mechanisms and the effect on the gait properties should also be investigated in the future.

References

1. T. McGeer, "Passive dynamic walking," *Int. J. Robot. Res.* **9**(2), 62–82 (Apr. 1990).
2. R. M. Alexander, *Principles of Animal Locomotion* (Princeton University Press, Princeton, NJ, USA, 2003).
3. T. McGeer, "Passive bipedal running," *Proc. R. Soc. Lond. Ser. B, Biol. Sci.* **240**(1297), 107–134 (May 1990).
4. M. Ahmadi and M. Buehler, "Stable control of a simulated one-legged running robot with hip and leg compliance," *IEEE Trans. Robot. Autom.* **13**(1), 96–104 (Feb. 1997).
5. F. Iida, J. Rummel and A. Seyfarth, "Bipedal Walking and Running with Compliant Legs," *Proceedings of the IEEE International Conference on Robotics and Automation* (Apr. 2007) pp. 3970–3975.
6. F. Asano, "Dynamic Gait Generation of Telescopic-Legged Rimless Wheel Based on Asymmetric Impact Posture," *Proceedings of the 9th IEEE-RAS International Conference on Humanoid Robots*, Paris, France (Dec. 2009) pp. 68–73.
7. F. Asano and M. Suguro, "High-Speed Dynamic Gait Generation Based on Forward Tilting Impact Posture Using Telescopic Legs and Forefeet," *Proceedings of the 13th International Conference on Climbing and Walking Robots and the Support Technologies for Mobile Machines (CLAWAR 2010)*, Nagoya, Japan (Sep. 2010) pp. 729–736.
8. F. Asano, "High-Speed Biped Gait Generation Based on Asymmetrization of Impact Posture Using Telescopic Legs," *Proceedings of the IEEE/RSJ International Conference on Intelligent Robots and Systems*, Taipei, Taiwan (Oct. 2010) pp. 4477–4482.
9. S. Collins, A. Ruina, R. Tedrake and M. Wisse, "Efficient bipedal robots based on passive-dynamic walkers," *Science* **307**(5712), 1082–1085 (Feb. 2005).
10. C. T. Farley, "Locomotion: Just skip it," *Nature* **394**, 721–723 (Aug. 1998).
11. A. E. Minetti, "The biomechanics of skipping gaits: A third locomotion paradigm?," *Proc. R. Soc. Lond. Ser. B, Biol. Sci.*, **265**(1402), 1227–1235 (Jul. 1998).
12. F. Asano and Z.-W. Luo, "On Energy-Efficient and High-Speed Dynamic Biped Locomotion with Semicircular Feet," *Proceedings of the IEEE/RSJ International Conference on Intelligent Robots and Systems*, Beijing, China (Oct. 2006) pp. 5901–5906.

https://doi.org/10.1017/S0263574711001226 Published online by Cambridge University Press